



Efficient photocatalytic CO₂ reduction over Co(II) species modified CdS in aqueous solution

Guixia Zhao^{a,1}, Wei Zhou^{b,1}, Yubing Sun^c, Xiangke Wang^c, Huimin Liu^a, Xianguang Meng^a, Kun Chang^a, Jinhua Ye^{a,b,d,*}

^a International Center for Materials Nanoarchitectonics (WPI-MANA), National Institute for Materials Science (NIMS), 1-1 Namiki, Tsukuba, Ibaraki 305-0044, Japan

^b TU-NIMS International Collaboration Laboratory, School of Material Science and Engineering, Tianjin University, 92 Weijin Road, Nankai District, Tianjin 300072, China

^c School of Environment and Chemical Engineering, North China Electric Power University, Beijing, 102206, China

^d Collaborative Innovation Center of Chemical Science and Engineering (Tianjin), Tianjin 300072, China



ARTICLE INFO

Keywords:
CO₂ reduction
Co(II) species
Aqueous solution
Configuration engineering

ABSTRACT

Efficient photocatalytic reduction of CO₂ into value-added chemical fuels has been a thorny, challenging and long-term project in the environmental/energy fields due to the low efficiency, especially in the inorganic aqueous environment. In this report, we present a facile approach to modify CdS with Co(II) species through controlling decarboxylation of the Co-EDTA precursor for improved CO₂ reduction. Performance evaluation and microstructure characterization reveal that the resulted tetra-coordinated Co(II) modified CdS exhibits the most optimized CO evolution rate of 9.8 μmol h⁻¹ (i.e., 392 μmol h⁻¹ g_(catalyst)⁻¹ with TOF of 7.94 h⁻¹) in aqueous solution under visible light, where the competitive hydrogen evolution reaction is significantly inhibited. Further investigation implies that the fully utilized Co(II) active sites, the tetra-coordinated Co(II) species, the favorable interaction between CO₂ and Co(II) sites and efficient charge transferring ensured the high efficiency and improved selectivity. This work would provide a good strategy for the structure engineering of catalytic site to improve photocatalytic CO₂ reduction.

1. Introduction

In the search trend to relieve the energy crisis and the increased panic from the climate change and sea levels-rising, photocatalytic CO₂ reduction has been considered as one of the most attractive routes to take advantage of the abundant solar energy and recycle CO₂ resource, mimicking the natural photosynthesis cycles for long-term CO₂ utilization [1–6]. To realize the ultimate goal, the challenging reductive half-reaction of CO₂ fixation needs to be well addressed, including increasing the efficiency and selectivity, especially minimizing the co-existed water reduction in the aqueous environment. Due to the chemical inert of linear CO₂, one-electron reduction of CO₂ to CO₂⁻ is highly unfavorable in thermodynamic with the standard potential of -1.9 V vs. NHE [7–9]. Although the proton assisted multi-electron reduction is substantially more favorable, suitable catalysts are still essential in the multi-proton and multi-electron reduction processes to decrease the kinetic resistance [10–16]. As reported by Ishitani and the coauthors, homogeneous system with Ru-based mononuclear or

multinuclear complexes exhibited prominent efficiency in the selective photocatalytic CO₂ reduction compared with the activity observed in heterogeneous system [17–19]. It is well-established that efficient electron transfer between the covalently linked photosensitizer and the catalytic sites, and the uniquely designed configuration of catalytic sites contribute to the outstanding performance [20–23]. More importantly, constructing homogeneously dispersed catalytic sites over semiconductor with selective and efficient catalytic activity would make up the gap between heterogeneous and homogeneous photocatalytic CO₂ reduction, with prospect of maintaining both high activity and long durability. Ru(II) complex was also successfully utilized as molecular catalyst combined with semiconductor for CO₂ reduction in the recent work by Ishitani [24,25]. However, the scarcity and high cost of Ru inspired the exploration for abundant transition metal-based alternative catalyst. To the best of our knowledge, structure engineering of transition metal catalyst anchored on semiconductor for selectively efficient CO₂ reduction in aqueous solution is still rare [17,26–32]. Since CdS has been widely used in visible-light photocatalysis with negative

* Corresponding author at: International Center for Materials Nanoarchitectonics (WPI-MANA), National Institute for Materials Science (NIMS), 1-1 Namiki, Tsukuba, Ibaraki 305-0044, Japan.

E-mail address: Jinhua.YE@nims.go.jp (J. Ye).

¹ These authors contributed equally to this work.

enough conduction band [33,34], herein, we first present a new strategy to anchor well-dispersed Co(II) species on CdS semiconductor support through controlling the decarboxylation of EDTA (ethylene-diaminetetraacetic acid) ligand in the Co-EDTA precursors during different-temperature calcination under argon, which resulted in one kind of tetra-coordinated Co(II) species that exhibits high efficiency toward CO₂ reduction into CO in aqueous solution with Na₂SO₃ as a sacrificial reductant under visible light irradiation, with a significantly inhibited hydrogen evolution rate.

2. Experimental section

2.1. Materials preparation

Ethylenediamine-*N,N,N',N'*-tetraacetic acid cobalt(II) disodium salt tetrahydrate (Co(II)-EDTA) was mixed with purchased CdS in different mole ratios (0.36%, 0.5%, 0.7%, 1.4%) in methanol solution by stirring at 60 °C for solvent evaporation. The default mole ratios of Co(II)-EDTA to CdS is 0.7%. The resulted mixture was calcinated at different temperatures (250, 275, 300, 350, 400 °C) under argon for 1 h and the obtained samples were referred to as CdS-CoE-x, in which x is the calcination temperature.

2.2. Characterization

Powder XRD was carried out on an X-ray diffractometer (Rint 2000, Altima III, Rigaku Co. Japan) with a Cu K α source. Thermogravimetric measurements were conducted on a Seiko Instrument thermogravimetry/differential thermal analyzer (TG-DTA 6200) under argon. Transmission electron microscopy (TEM) images, combined with energy dispersive X-ray spectroscopy (EDS) mapping were recorded with a field emission transmission electron microscope (JEM2100F, JEOL Co., Japan) operating at 200 kV. FT-IR spectra were recorded by Nicolet 4700 spectrometer with reflection mode. XPS measurement was carried out with electron spectrometer (PHI Quantera SXM, ULVAC-PHI Inc., Japan). The UV-vis absorption was measured with a UV-vis spectrophotometer (Shimadzu, UV-2600) using BaSO₄ as the reflectance standard reference. ESR measurements were carried out at room temperature on a JEOL JES-FA-200. PL spectra were recorded by a JASCO FP-6500 spectrofluorometer. The fluorescence decay curve was measured using a compact fluorescence lifetime spectrometer (Quantaurus-Tau, C11367), excited at 420 nm. EXAFS signals of the Co K-edge were recorded at 14 W1 beamline of the Shanghai Synchrotron Radiation Facility (SSRF, China) in the fluorescence mode for CdS-CoE-x samples and in the transmission mode for Metallic cobalt and cobalt sulfide. The electron beam energy was 3.5 GeV with the mean stored current was 300 mA. The energy of the X-ray was tuned using a fixed-exit double-crystal Si (111) monochromator. Metallic cobalt foil and cobalt sulfide were used for energy calibration and as references. The intensities of the incident and fluorescence X-ray were monitored by using standard N₂-filled ion chamber and Ar-filled Lytle-type detector, respectively. Analysis of the obtained EXAFS data was performed using Athena and Artemis interfaces to the IFFEFIT software. All fits were performed in the R space with k-weight of 3.

2.3. Photocatalytic activity evaluation

Photocatalytic activities were evaluated by the CO₂ reduction from aqueous solution containing Na₂CO₃ under visible light irradiation with sodium sulfite as electron donor. In detail, the 25 mg catalyst and 70 mL of Na₂CO₃ and Na₂SO₃ solution (0.3 mol/L and 0.06 mol/L) were added in a Pyrex glass reaction cell which was connected to a gas-closed system with a gas-circulated pump. Before the irradiation, the reaction cell was evacuated to remove the air completely. And then 80 kPa of pure CO₂ was inlet into the reaction cell. A 300 W xenon arc lamp with a UV-cut filter (to remove light with wavelength lower than 420 nm)

was used as light source. The produced CO was analyzed by an online gas chromatograph (GC-8A, Shimadzu Corp., Japan). The isotope test was carried out by using ¹³CO₂ dissolved in NaOH as carbon source with the same reaction set as mentioned above and the gas products were analyzed by gas chromatography-mass spectrometry (JEOL-GCQMS, JMS-K9 and 6890N Network GC system, Agilent Technologies). The apparent quantum efficiency (AQE) at 420 nm was calculated by the following equation: AQE = (2 × amount of CO molecules evolved in unit time/number of incident photons in unit time) × 100%.

2.4. Computational methods

All calculations were carried out with VASP (Vienna ab initio simulation package) code based on the density functional theory (DFT). The generalized gradient approximation (GGA) was used for the exchange-correlation energy. A plane-wave expansion for the basis set with a cutoff energy of 450 eV was employed. 2 × 2 × 1 Monk-horst k-point meshes was used for the Brillouin-zone integrations of the slab model, respectively. All atoms are relaxed until the residual Hellmann-Feynman force was less than 0.04 eV/Å. Moreover, the convergence for energy is chosen as 10⁻⁵ eV.

3. Results and discussion

EDTA is widely used as a chelating agent for transition metal ions like Ni²⁺, Co²⁺, to form hexadentate metal-EDTA complex. We utilize the Co-EDTA decomposition for the chemical anchoring of Co(II) species on the CdS surface through calcination the mixture of CdS and Co-EDTA (with the mole proportion of Co-EDTA to CdS equals to 0.7%) at different temperatures as illustrated in Fig. 1, resulting in the CdS-CoE-x (x represent the calcination temperature). Decarboxylation of the carboxylate groups in Co-EDTA can be inferred from the decreased absorbance at around 1700, 1400 and 1100 cm⁻¹ in the *in situ* FTIR spectra, as well as the emerged CO₂ signal at 2350 cm⁻¹ originated from the gaseous phase. After calcination under 350 °C for 1 h, the resulted CdS-CoE-350 consists a thin layer on the surface of CdS as shown in the HRTEM image, without forming visible nanoparticles (Fig. 1). The uniform dispersion of Co element is confirmed from the energy-dispersive x-ray spectroscopy (EDS) analysis mapping in scanning transmission electron microscope (STEM) (inset of Fig. 1 and Fig. S1). TEM and HRTEM images of the resultant samples from other calcination temperatures such as CdS-CoE-300 and CdS-CoE-400 are shown in Fig. S2, in which, similar thin layer is found in CdS-CoE-300, while small nanoparticles are formed in CdS-CoE-400.

The x-ray diffraction pattern (XRD) (Fig. S3a) also confirmed the maintained pure hexagonal phase of CdS with P63mc space group for all the Co modified CdS. FT-IR absorption spectrum of CdS-CoE-x in Fig. S3b exhibit the signals at 1148, 880, 1452 and 1600–1700 cm⁻¹, proving the existence of C–N, Co–N, –CH₂– and COO[–], with decreased absorbance from COO[–] at elevated temperature. It is inferred that COO[–], C–N and –CH₂– groups from EDTA ligands can be reserved under moderate calcination. The UV-vis diffuse reflectance spectra (Fig. 2) show that CdS-CoE-x samples have similar absorption edges to pure CdS, although with slightly increased absorption toward visible light caused by the fluctuation of background noise. X-ray photoelectron spectroscopy (XPS) (Fig. S4) confirmed the presence of C, N and the similar Co(II) state in CdS-CoE-x.

To further verify the microstructure of the Co(II) species on CdS-CoE-350 and the Co(II) structure difference between CdS-CoE-350 and CdS-CoE-300, the X-ray absorption near-edge structure (XANES) spectroscopy and the Co K-edge extended x-ray absorption fine structure (EXAFS) spectrometry were utilized. The overall profile of the Co K-edge XANES spectra of CdS-CoE-300 and CdS-CoE-350 are obviously different from those of metallic Co and CoS (Fig. S5), suggesting a disparate Co location environment. As shown in the EXAFS Fourier

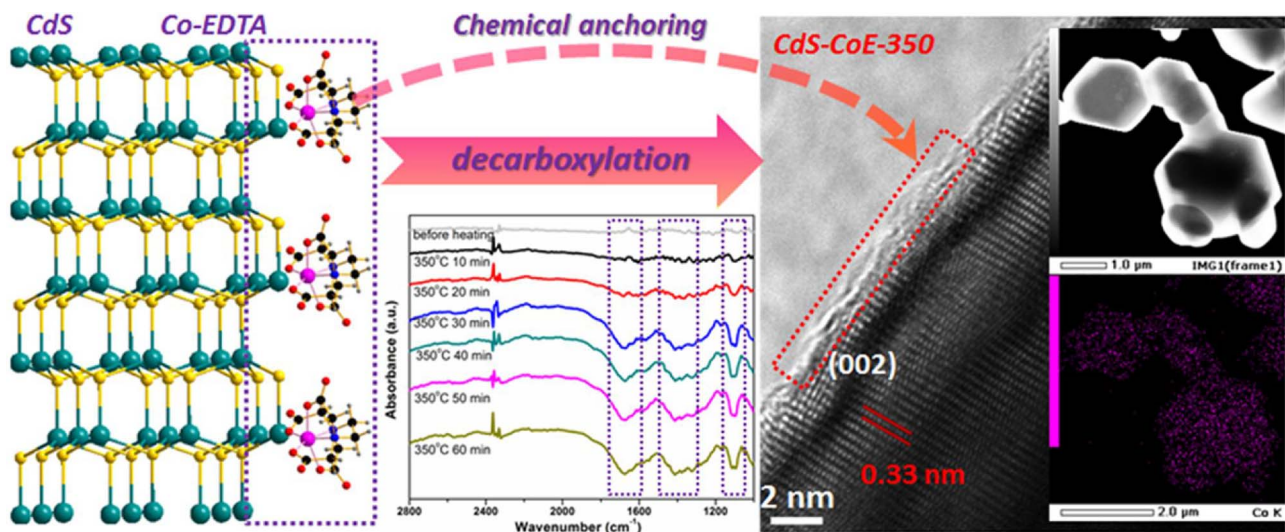


Fig. 1. Schematic illustration for the chemical anchoring of the Co species on the CdS surface through the controlled decomposition of Co-EDTA precursor. Middle: *in situ* FTIR spectra measured during the calcination of Co-EDTA at 350 °C; Right: HRTEM of resulted CdS-CoE-350; inset: STEM image and EDS elemental mapping of CdS-CoE-350.

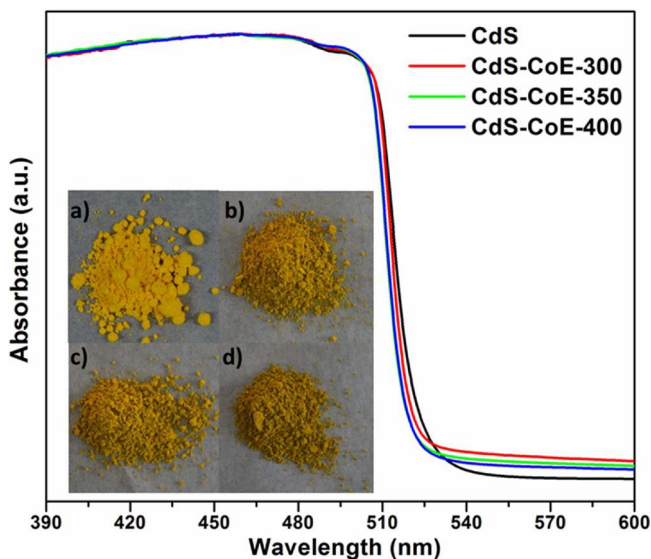


Fig. 2. UV-vis diffuse reflectance spectra of pure CdS, CdS-CoE-x; inset: photograph of CdS (a) and CdS-CoE-x samples (b: CdS-CoE-300; c: CdS-CoE-350; d: CdS-CoE-400).

Transforms (FTs) in Fig. 3a, the scattering peaks in the low R-position range of 1–2.2 Å for CdS-CoE-350 can be fitted as the result of the scattering pairs of Co-N(O) and Co-S [35,36]. As referenced samples, CoS and Co foil exhibit obviously different radial structural functions (RSFs) spectra, which contain the typical Co-S and Co-Co scattering pair in the first shell, respectively. The EXAFS fitting results in Table S1 confirmed that the local Co(II) in CdS-CoE-350 is coordinated with nitrogen(oxygen) and sulfur atoms, with the respective coordination number of surrounding nitrogen(oxygen) and sulfur atoms close to 2, which means Co(II) in CdS-CoE-350 is tetra-coordinated on the CdS surface, although O and N can't be distinguished. While for CdS-CoE-300, the Co K-edge EXAFS Fourier Transform (Fig. S6) shows asymmetrical scattering peaks with R-space from 1.0 to 2.1 Å, which can be assigned well to the scattering shells of Co-O(N), Co-N(O) and Co-S. The EXAFS fitting results indicated that the local Co(II) in CdS-CoE-300 is coordinated with 2-oxygen, 2-nitrogen and 1-sulfur atoms in the distance of 1.45, 1.59 and 1.89 Å, respectively, which means Co(II) in CdS-CoE-300 is penta-coordinated on the CdS surface [37]. In brief, Co(II) could be attached on CdS through coordination with edged sulfur from CdS, forming a penta-coordinated structure and a tetra-coordinated

structure, at 300 °C and 350 °C respectively. In summary of the above, it is concluded that different discrete Co(II) species can be planted on the surface of CdS through bonding with the surface unsaturated sulfur, as a result of the controlled decarboxylation of EDTA ligands, instead of forming the continuous extended structure in nanoparticles. Thermo-gravimetry analysis (TGA) was used to further track the decomposition of Co-EDTA in the mixture with CdS during the calcination at 300 °C and 350 °C. As indicated in the weight loss curves (Fig. S7), 0.53% of weight loss during the 1 h-calcination at 300 °C indicates an estimated two CO₂ molecules releasing for every Co-EDTA molecule, while 0.99% of weight loss after 1 h-calcination at 350 °C suggested around four CO₂ units releasing for every Co-EDTA molecule. Such stepwise decarboxylation agrees well with the FTIR results (Fig. S3b) mentioned above.

CO₂ reduction activity was evaluated in Na₂CO₃/Na₂SO₃ solution saturated with atmospheric CO₂ under visible light ($\lambda > 420$ nm) in a closed gas circulation system [1]. Fig. 4a–b showed the time course of CO/H₂ evolution over pure CdS and CdS-CoE-x. Surprisingly, CdS-CoE-350 showed the highest CO evolution rate of 9.8 μmol h⁻¹ (i.e., 392 μmol h⁻¹ g⁻¹ catalyst) and the lowest H₂ evolution rate of 46.1 μmol h⁻¹, with a selectivity of 17.5%, while CdS-CoE-300 exhibited the highest H₂ evolution rate of 917.2 μmol h⁻¹ and low CO evolution rate of 0.3 μmol h⁻¹ (Fig. 4c). Cycling testing (Fig. 4d) indicated that the CO evolution over CdS-CoE-350 is stable with the TOF (towards the Co sites) of 7.94 h⁻¹. Isotope experiment was carried out to validate the source of generated CO by using ¹³CO₂ as carbon source resolved in NaOH solution to form Na₂CO₃. As shown in Fig. S8, the peak at *m/z* = 29 indicated that the produced ¹³CO indeed originated from ¹³CO₂ species in the aqueous solution. A comparison of various cocatalyst for CO₂ reduction suggested that the CO evolution rate of CdS-CoE-350 is 42 times, 13 times and 23 times as high as that of pure CdS, CdS loaded with CoCl₂ as cocatalyst precursor, and CdS loaded Pt, respectively (Fig. 4e). To estimate the real performance of photocatalysts, we investigated the apparent quantum efficiency (AQE) of CdS-CoE-350 for CO evolution at 420 nm, which turned out to be 2.2% as listed in Table S2, also outperforming most photocatalysis systems although still quite low compared with that for the photocatalytic hydrogen evolution [38,39]. More importantly, the selectivity of CO₂ reduction over water reduction on CdS-CoE-350 is far higher than on other kinds of catalyst like CdS-CoE-300, pure CdS, CdS loaded with CoCl₂ as cocatalyst precursor, and CdS loaded Pt as shown in Fig. 4c and e. The effect of loaded Co-EDTA ratio on CdS to the CO₂ reduction on CdS-CoE-350 is also investigated. As shown in Fig. 4f, the hybrid with loaded 0.7% mole proportion of Co-EDTA shows the highest CO

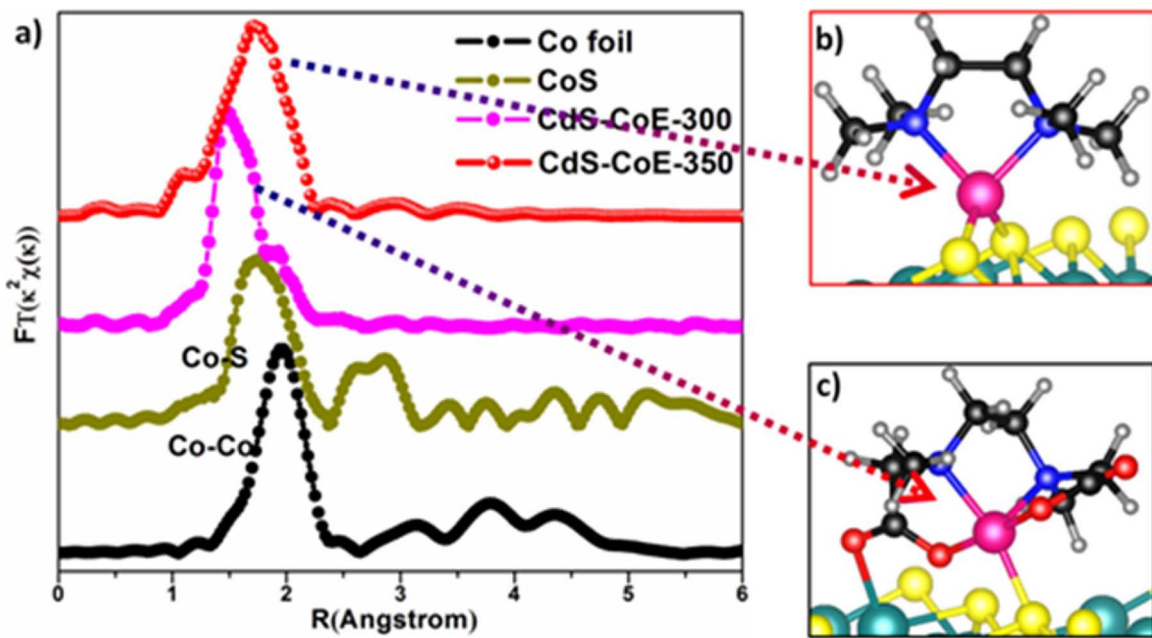


Fig. 3. a) Fourier transform magnitudes of the experimental Co K-edge EXAFS spectra of CdS-CoE and the referenced samples; b and c) the proposed structure of Co species attached on CdS according to the EXAFS fitting results and the DFT modeling.

evolution rate and selectivity, implying that the appropriate amount of Co-EDTA precursor is critical for the dispersion of molecule Co(II) species and the balance between the CO_2 reduction and competitive H_2O reduction in the resulted CdS-CoE-350. To exclude the possibility of the cocatalysis by the decomposed EDTA, referenced sample prepared by calcination of CdS and EDTA mixture at 350 °C was conducted for the photocatalytic CO_2 reduction. None of CO can be detected after 10 h-irradiation, suggesting that the Co(II) is the catalytic center for CO_2 reduction.

In situ electron spin resonance (ESR) measurement was then carried out to unveil the mechanism in the photocatalytic process. To avoid the solvent effect, we collected the ESR signal of IPA-infiltrated CdS-CoE hybrids with and without irradiation under visible light. It shows in Fig.

S9 that in dark condition, CdS-CoE-300 and CdS-CoE-350 showed a broad resonance at $g = 2.3066$ and 2.3085, respectively, while under irradiation, both of the signals largely weakened. Considering the diamagnetism of Co(I) species, it is reasonable to attribute the weakened signals to the efficient electron trapping by the Co(II) on the surface of CdS-CoE-300 and CdS-CoE-350 [22,40]. We further tried to disclose the original cause for the large gap between the activity of CdS-CoE-300 and CdS-CoE-350. The quenched photoluminescence suggested a decreased electron-hole recombination in CdS-CoE-x than that in pure CdS (Fig. 5) [41]. It is proposed that in CdS-CoE-300 and CdS-CoE-350, the electron-hole recombination is largely prevented due to the efficient electron trapping by the Co(II).

However, there is still no adequate support for the large difference

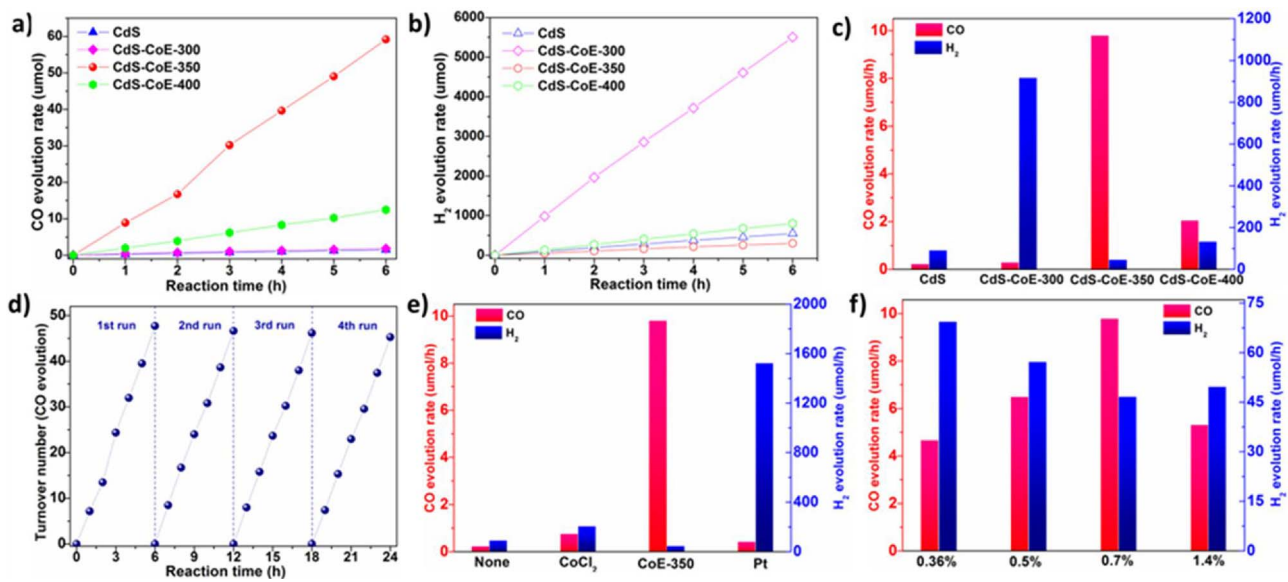


Fig. 4. (a-b) Time-dependent CO and H_2 evolution in the photocatalytic CO_2 reduction with the presence of Na_2CO_3 and Na_2SO_3 over pure CdS, and CdS-CoE-x prepared in different temperatures with 0.7% of initial mole proportion of Co-EDTA to CdS; (c) the comparison of CO and H_2 evolution rate over pure CdS, and CdS-CoE-x (d) Cycling test of CO evolution in the photocatalytic CO_2 reduction over CdS-CoE-350; (e) the comparison of CO and H_2 evolution rate over Cds with different kinds of cocatalyst; (f) CO and H_2 evolution rate over CdS-CoE-350 with various initial mole proportions of Co-EDTA to CdS in the CdS and Co-EDTA mixtures. Light source: 300-W Xe lamp with L42cut-off; Reaction condition: 70 mL of Na_2CO_3 (0.3 mol/L) and Na_2SO_3 solution (0.06 mol/L); Catalyst: 25 mg.

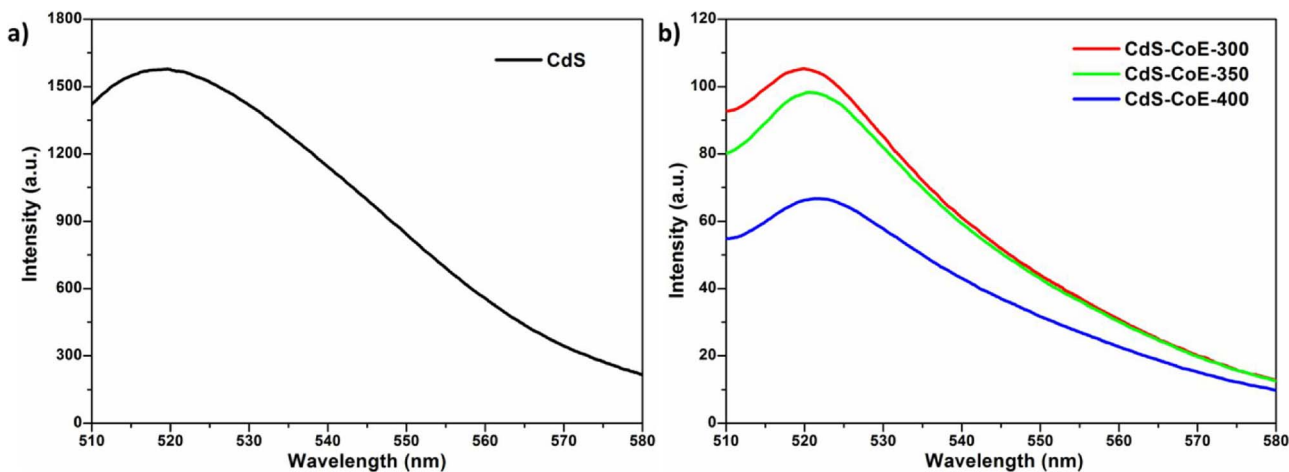
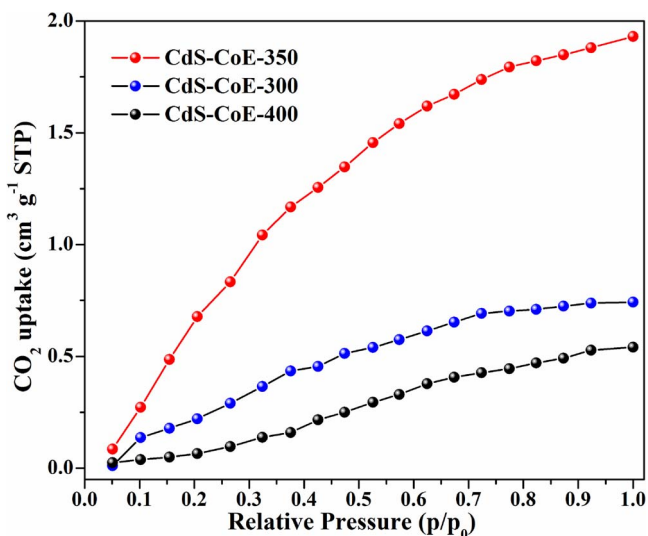


Fig. 5. Photoluminescence spectra of CdS and CdS-CoE-x under 420 nm excitation.

Fig. 6. CO₂ adsorption behaviors for CdS-CoE-300, CdS-CoE-350 and CdS-CoE-400.

of CO₂ reduction selectivity between CdS-CoE-300 and CdS-CoE-350 according to the above analysis. Further investigation is focused on the spatial Co(II) structure in CdS-CoE-300 and CdS-CoE-350. DFT calculation was utilized to monitor the most stable distribution of Co(II) species as shown in Fig. 3b and c. It is speculated that the different Co (II) configurations would exhibit different spatial favor to the attachment of CO₂. Herein, we used the volumetric CO₂ adsorption measurement to investigate the interaction between carbonate ions and the CdS-CoE-300, CdS-CoE-350 and CdS-CoE-400 surface. As shown in Fig. 6, CdS-CoE-400 showed the lowest affinity and CdS-CoE-300 showed a little higher, while the CdS-CoE-350 exhibited 2.6-fold increased CO₂ adsorption amount compared with CdS-CoE-300. Considering the microstructure characterization results of the Co(II) species on CdS-CoE-350 and CdS-CoE-300 by XANES and EXAFS, it is concluded that the tetra-coordinated structure of Co²⁺ shows much higher affinity than the penta-coordinated structure of Co²⁺. We also found out similar high CO₂ affinity in tetra-coordinated Co²⁺ in cobalt-porphyrin in our previous work [37], which helps to understand the cause for the best performance of CdS-CoE-350 toward CO₂ reduction. In brief of the above discussion, the efficient and relatively selective CO₂ reduction in aqueous solution can be contributed to well-dispersed Co(II) active sites, the efficient charge transferring, and crucially, the favorable tetra-coordination of Co(II) species in CdS-CoE-350.

4. Conclusions

In conclusion, we have introduced a facile strategy to plant well-dispersed Co(II) species on the CdS surface through the controlled decomposition of Co-EDTA precursors. The resulted CdS-CoE-350, with a tetra-coordinated Co(II) species on the surface, exhibits a selective CO₂ reduction in HCO₃⁻ aqueous solution, reaching an efficient photocatalytic CO evolution rate of 9.8 μmol h⁻¹ (i.e., 392 μmol h⁻¹ g_(catalyst)⁻¹) with a TOF of 7.94 h⁻¹. It was found out that the coordinated configuration of cocatalyst plays an important role in the interaction between CO₂ and active sites. The fully utilized Co(II) active sites, special tetra-coordination of Co(II) and the efficient charge transferring contribute to the excellent photocatalytic CO₂ reduction. It is proposed that such kind precursor is promising to construct well-dispersed and active transition metal to maximize the catalytic efficiency.

Acknowledgements

This work received financial support from the National Basic Research Program of China (973 Program, 2014CB239301), JSPS Postdoctoral Fellowship for Foreign Researchers, the World Premier International Research Center Initiative (WPI Initiative) on Materials Nano-architectonics (MANA), MEXT (Japan) and the National Natural Science Foundation of China (21633004). The authors also thank beamline BL14W1 (Shanghai Synchrotron Radiation Facility) for providing the beam time. The authors acknowledge the technical support from Dr. Toshiaki Takei and Dr. Bo Da.

Appendix A. Supplementary data

Supplementary data associated with this article can be found, in the online version, at <https://doi.org/10.1016/j.apcatb.2017.12.054>.

References

- [1] X. Meng, Q. Yu, G. Liu, L. Shi, G. Zhao, H. Liu, P. Li, K. Chang, T. Kako, J. Ye, Efficient photocatalytic CO₂ reduction in all-inorganic aqueous environment: co-operation between reaction medium and Cd(II) modified colloidal ZnS, *Nano Energy* 34 (2017) 524–532.
- [2] H. Tong, S.X. Ouyang, Y.P. Bi, N. Umezawa, M. Oshikiri, J.H. Ye, Nano-photocatalytic materials: possibilities and challenges, *Adv. Mater.* 24 (2012) 229–251.
- [3] Y.H. Fu, D.R. Sun, Y.J. Chen, R.K. Huang, Z.X. Ding, X.Z. Fu, Z.H. Li, An amine-functionalized titanium metal-Organic framework photocatalyst with visible-light-Induced activity for CO₂ reduction, *Angew. Chem. Int. Edit.* 51 (2012) 3364–3367.
- [4] Y. Izumi, Recent advances in the photocatalytic conversion of carbon dioxide to fuels with water and/or hydrogen using solar energy and beyond, *Coord. Chem. Rev.* 257 (2013) 171–186.
- [5] H. Liu, M. Li, T.D. Dao, Y. Liu, W. Zhou, L. Liu, X. Meng, T. Nagao, J. Ye, Design of

PdAu alloy plasmonic nanoparticles for improved catalytic performance in CO₂ reduction with visible light irradiation, *Nano Energy* 26 (2016) 398–404.

[6] G. Zhao, X. Huang, X. Wang, X. Wang, Progress in catalyst exploration for heterogeneous CO₂ reduction and utilization: a critical review, *J. Mater. Chem. A* 5 (2017) 21625–21649.

[7] H. Schwarz, R. Dodson, Reduction potentials of CO₂ and the alcohol radicals, *J. Phys. Chem.* 93 (1989) 409–414.

[8] S.C. Yan, S.X. Ouyang, J. Gao, M. Yang, J.Y. Feng, X.X. Fan, L.J. Wan, Z.S. Li, J.H. Ye, Y. Zhou, A room-temperature reactive-template route to mesoporous ZnGa₂O₄ with improved photocatalytic activity in reduction of CO₂, *Angew. Chem.* 122 (2010) 6544–6548.

[9] W. Tu, Y. Zhou, Z. Zou, Photocatalytic conversion of CO₂ into renewable hydrocarbon fuels: state-of-the-art accomplishment, challenges, and prospects, *Adv. Mater.* 26 (2014) 4607–4626.

[10] W. Kim, B.A. McClure, E. Edri, H. Frei, Coupling carbon dioxide reduction with water oxidation in nanoscale photocatalytic assemblies, *Chem. Soc. Rev.* 45 (2016) 3221–3243.

[11] H. Shi, G. Chen, C. Zhang, Z. Zou, Polymeric g-C₃N₄ coupled with NaNbO₃ nanowires toward enhanced photocatalytic reduction of CO₂ into renewable fuel, *ACS Catal.* 4 (2014) 3637–3643.

[12] X. An, K. Li, J. Tang, Cu₂O/reduced graphene oxide composites for the photocatalytic conversion of CO₂, *ChemSusChem* 7 (2014) 1086–1093.

[13] G.G. Zhang, Z.A. Lan, X.C. Wang, Merging surface organometallic chemistry with graphitic carbon nitride photocatalysis for CO₂ photofixation, *ChemCatChem* 7 (2015) 1422–1423.

[14] J.L. Lin, Z.M. Pan, X.C. Wang, Photochemical reduction of CO₂ by graphitic carbon nitride polymers, *ACS Sustain. Chem. Eng.* 2 (2014) 353–358.

[15] H. Zhou, P. Li, J. Liu, Z. Chen, L. Liu, D. Dontsova, R. Yan, T. Fan, D. Zhang, J. Ye, Biomimetic polymeric semiconductor based hybrid nanosystems for artificial photosynthesis towards solar fuels generation via CO₂ reduction, *Nano Energy* 25 (2016) 128–135.

[16] T.M. Suzuki, T. Takayama, S. Sato, A. Iwase, A. Kudo, T. Morikawa, Enhancement of CO₂ reduction activity under visible light irradiation over Zn-based metal sulfides by combination with Ru-complex catalysts, *Appl. Catal. B-Environ.* 224 (2018) 572–578.

[17] S. Sato, T. Morikawa, T. Kajino, O. Ishitani, A highly efficient mononuclear iridium complex photocatalyst for CO₂ reduction under visible light, *Angew. Chem.* 125 (2013) 1022–1026.

[18] B. Gholamkhass, H. Mametsuka, K. Koike, T. Tanabe, M. Furue, O. Ishitani, Architecture of supramolecular metal complexes for photocatalytic CO₂ reduction: ruthenium-rhenium bi- and tetrานuclear complexes, *Inorg. Chem.* 44 (2005) 2326–2336.

[19] Y. Tamaki, T. Morimoto, K. Koike, O. Ishitani, Photocatalytic CO₂ reduction with high turnover frequency and selectivity of formic acid formation using Ru(II) multinuclear complexes, *Proc. Natl. Acad. Sci.* 109 (2012) 15673–15678.

[20] A. Nakada, K. Koike, T. Nakashima, T. Morimoto, O. Ishitani, Photocatalytic CO₂ reduction to formic acid using a Ru(II)-Re(I) supramolecular complex in an aqueous solution, *Inorg. Chem.* 54 (2015) 1800–1807.

[21] H. Huang, J. Lin, G. Zhu, Y. Weng, X. Wang, X. Fu, J. Long, A long-Lived mononuclear cyclopentadienyl ruthenium complex grafted onto anatase TiO₂ for efficient CO₂ photoreduction, *Angew. Chem.* 128 (2016) 8454–8458.

[22] G.X. Zhao, H. Pang, G.G. Liu, P. Li, H.M. Liu, H.B. Zhang, L. Shi, J.H. Ye, Co-porphyrin/carbon nitride hybrids for improved photocatalytic CO₂ reduction under visible light, *Appl. Catal. B-Environ.* 200 (2017) 141–149.

[23] L. Lin, C. Hou, X. Zhang, Y. Wang, Y. Chen, T. He, Highly efficient visible-light driven photocatalytic reduction of CO₂ over g-C₃N₄ nanosheets/tetra(4-carboxyphenyl)porphyrin iron(III) chloride heterogeneous catalysts, *Appl. Catal. B-Environ.* 221 (2018) 312–319.

[24] R. Kuriki, K. Sekizawa, O. Ishitani, K. Maeda, Visible-light-driven CO₂ reduction with carbon nitride: enhancing the activity of ruthenium catalysts, *Angew. Chem. Int. Ed.* 54 (2015) 2406–2409.

[25] K. Sekizawa, K. Maeda, K. Domen, K. Koike, O. Ishitani, Artificial Z-scheme constructed with a supramolecular metal complex and semiconductor for the photocatalytic reduction of CO₂, *J. Am. Chem. Soc.* 135 (2013) 4596–4599.

[26] R. Kuriki, H. Matsunaga, T. Nakashima, K. Wada, A. Yamakata, O. Ishitani, K. Maeda, Nature-inspired, highly durable CO₂ reduction system consisting of a binuclear ruthenium (II) complex and an organic semiconductor using visible light, *J. Am. Chem. Soc.* 138 (2016) 5159–5170.

[27] R. Kuriki, K. Sekizawa, O. Ishitani, K. Maeda, Visible-light-driven CO₂ reduction with carbon nitride: enhancing the activity of ruthenium catalysts, *Angew. Chem. Int. Ed.* 54 (2015) 2406–2409.

[28] H.-Q. Xu, J. Hu, D. Wang, Z. Li, Q. Zhang, Y. Luo, S.-H. Yu, H.-L. Jiang, Visible-light photoreduction of CO₂ in a metal-organic framework: boosting electron-hole separation via electron trap states, *J. Am. Chem. Soc.* 137 (2015) 13440–13443.

[29] J. Lin, Z. Pan, X. Wang, Photochemical reduction of CO₂ by graphitic carbon nitride polymers, *ACS Sustain. Chem. Eng.* 2 (2013) 353–358.

[30] S. Wang, X. Wang, Imidazolium ionic liquids imidazolylidene heterocyclic carbenes, and zeolitic imidazolate frameworks for CO₂ capture and photochemical reduction, *Angew. Chem. Int. Ed.* 55 (2016) 2308–2320.

[31] Y. Oh, X. Hu, Organic molecules as mediators and catalysts for photocatalytic and electrocatalytic CO₂ reduction, *Chem. Soc. Rev.* 42 (2013) 2253–2261.

[32] A. Iwase, S. Yoshino, T. Takayama, Y.H. Ng, R. Amal, A. Kudo, Water splitting and CO₂ reduction under visible light irradiation using Z-scheme systems consisting of metal sulfides CoO_x-loaded BiVO₄, and a reduced graphene oxide electron mediator, *J. Am. Chem. Soc.* 138 (2016) 10260–10264.

[33] T.-T. Yang, W.-T. Chen, Y.-J. Hsu, K.-H. Wei, T.-Y. Lin, T.-W. Lin, Interfacial charge carrier dynamics in core-shell Au-CdS nanocrystals, *J. Phys. Chem. C* 114 (2010) 11414–11420.

[34] Y.-F. Lin, Y.-J. Hsu, Interfacial charge carrier dynamics of type-II semiconductor nanoheterostructures, *Appl. Catal. B-Environ.* 130–131 (2013) 93–98.

[35] H. Fei, J. Dong, M.J. Arellano-Jiménez, G. Ye, N.D. Kim, E.L. Samuel, Z. Peng, Z. Zhu, F. Qin, J. Bao, Atomic cobalt on nitrogen-doped graphene for hydrogen generation, *Nat. Commun.* 6 (2015) 8668.

[36] G. Zhao, Y. Sun, W. Zhou, X. Wang, K. Chang, G. Liu, H. Liu, T. Kako, J. Ye, Superior photocatalytic H₂ production with cocatalytic Co/Ni species anchored on sulfide semiconductor, *Adv. Mater.* 29 (2017) 1703258.

[37] H.B. Zhang, J. Wei, J.C. Dong, G.G. Liu, L. Shi, P.F. An, G.X. Zhao, J.T. Kong, X.J. Wang, X.G. Meng, J. Zhang, J.H. Ye, Efficient visible-light-driven carbon dioxide reduction by a single-atom implanted metal-organic framework, *Angew. Chem. Int. Edit.* 55 (2016) 14308–14312.

[38] J. Yu, J. Low, W. Xiao, P. Zhou, M. Jaroniec, Enhanced photocatalytic CO₂-reduction activity of anatase TiO₂ by coexposed {001} and {101} facets, *J. Am. Chem. Soc.* 136 (2014) 8839–8842.

[39] S.B. Wang, X.C. Wang, Photocatalytic CO₂ reduction by CdS promoted with a zeolitic imidazolate framework, *Appl. Catal. B-Environ.* 162 (2015) 494–500.

[40] J.G. McAlpin, Y. Surendranath, M. Dincă, T.A. Stich, S.A. Stoian, W.H. Casey, D.G. Nocera, R.D. Britt, EPR evidence for Co(IV) species produced during water oxidation at neutral pH, *J. Am. Chem. Soc.* 132 (2010) 6882–6883.

[41] E.A. Medlycott, G.S. Hanan, Synthesis and properties of mono-and oligo-nuclear Ru (II) complexes of tridentate ligands: the quest for long-lived excited states at room temperature, *Coord. Chem. Rev.* 250 (2006) 1763–1782.